CHAPTER 4

Estimation of ionospheric total electron content (TEC) from GNSS observations

Gopi Krishna Seemala
Indian Institute of Geomagnetism, Navi Mumbai, India

4.1 Introduction

In the early days of radio, mathematical physicists theoretically proved by that even for very long waves it will be impossible to receive radio signals at long distances beyond curvature of earth because of the diffractive attenuation. In 1882, Balfour Stewart in his studies of earth's magnetism [1], discovered that diurnal variation of magnetic field can be explained by currents in the upper atmosphere. However, in 1901 Guglielmo Marconi demonstrated the reception of long-distance radio signals across the Atlantic Ocean, that is, around an appreciable portion of the curved earth. That stimulated widespread interest in the studies of this phenomenon. The following year, Kennelly [2] and Heaviside [3] independently postulated that the earth is surrounded by an ionized atmospheric layer which acts as a reflector and so prevents the wave from escaping into space; to explain the long-distance radio transmission at a time when others were investigating diffraction effects as an explanation. The first direct experimental evidence for the existence of an ionized region was obtained by Appleton and Barnett [4], with the "frequency change" experiments using the BBC transmitter at Bournemouth. They measured the arrival angle of waves from a distant transmitter and showed that they arrived at an elevated angle, that is, that there is a "sky-wave." Experiments of this kind indicated that the heights of reflection were of the order of 100–200 km. Subsequent work has demonstrated the existence of several well-defined ionized regions, and of rather complicated layer structure within each. The name "ionosphere" for these ionized regions of atmosphere was suggested by Watson-Watt, and was universally adopted.

Earlier, the ionospheric research was mostly carried out by radio engineers as they are motivated by the need to improve long-range radio communication. Then, subsequently, the focus shifted to understanding the effects of ionosphere on satellites as they orbit in this ionized medium. Today, we have vast scientific knowledge of the ionosphere owing to the amount of data generated from satellite remote sensing, and was enhanced by progress in theoretical and laboratory experimental techniques.

Thus, the ionosphere is a part of earth's upper atmospheric shell where the electrons and ionized atoms and molecules, that spans from an altitude of about 50 km to more than 1000 km. In the ionosphere, the charged particles or electrons and ions are

Atmospheric Remote Sensing
DOI: https://doi.org/10.1016/B978-0-323-99262-6.00022-5

created by the photo-ionization due to solar radiation incidence on neutral atoms and molecules of air. This ionization occurs primarily due to ultraviolet radiation (UV) and X-rays from the sun. The ionosphere can conduct electrical currents as well as reflect, deflect, and scatter radio waves. In general, ionosphere has a lower altitude limit of about 50–70 km and there is no distinct upper limit, but in most studies and for application purposes the upper limit is kept at 2000 km. At higher altitudes of ionosphere, the region is called magnetosphere which extends from about several hundred kilometers from earth's surface to tens of thousands of kilometers into space. In this region, the charged particle's behavior is strongly influenced by the magnetic fields of both earth and sun. The maximum electron density of the ionosphere is usually observed at an altitude of about 300 km, where only a tiny fraction (<1%) of neutral atmospheric gas is ionized.

4.1.2 Ionospheric layers

It is well known that atmospheric density reduces with height due to the gravity of the earth, and this vertical gradient is much larger than the horizontal gradient. The simplest type of ionized layer that can be considered theoretically is the so-called "Chapman layer," [5]. Suppose ultra-violet or X-ray radiation of a wave-length with enough photon energy for photo-ionization of an atmospheric gas is incident on atmosphere, whose density and absorption coefficient, vary exponentially with altitude. As the radiation goes deeper into the atmosphere, it gets absorbed more and the radiation intensity is decreased. At a sufficiently low height the greater part of the radiation is absorbed, and a lower bound is formed to the region of ionization produced by the radiation. This results in a region with maximum density of ionization called a Chapman layer. The actual ionization density present at any given time will represent a balance between the rates of production, accumulation, and loss.

Practically, the ionosphere has more complicated structure than a single layer of ionization, as there are several gases present in the atmosphere and their concentrations vary differently with height. The most abundant gas molecules that are ready for ionization due to incident solar radiation are molecular oxygen (O_2) and nitrogen (N_2) below 200 km; atomic oxygen (O) above 200 km, and hydrogen (H) and Helium (He) above 600 km altitude (for more details refer to Fig. 1.2 in [6]). The different gases need different wavelengths of radiation to get ionized. The resultant plasma density is a balance between the rate at which electrons are produced and the rate at which they are lost. The electrons and ions are lost mostly due to recombination and diffusion. These rates of recombination and diffusion change with altitude. This altitudinal variation of electron production and recombination rates creates a density profile with altitude, and results in several distinct layers (D, E, and F). Now it is known that these layers are not so distinct as earlier thought. Edward V. Appleton, who studied ionosphere extensively by radio probing it, is the one who brought this nomenclature. Initially, when he studied

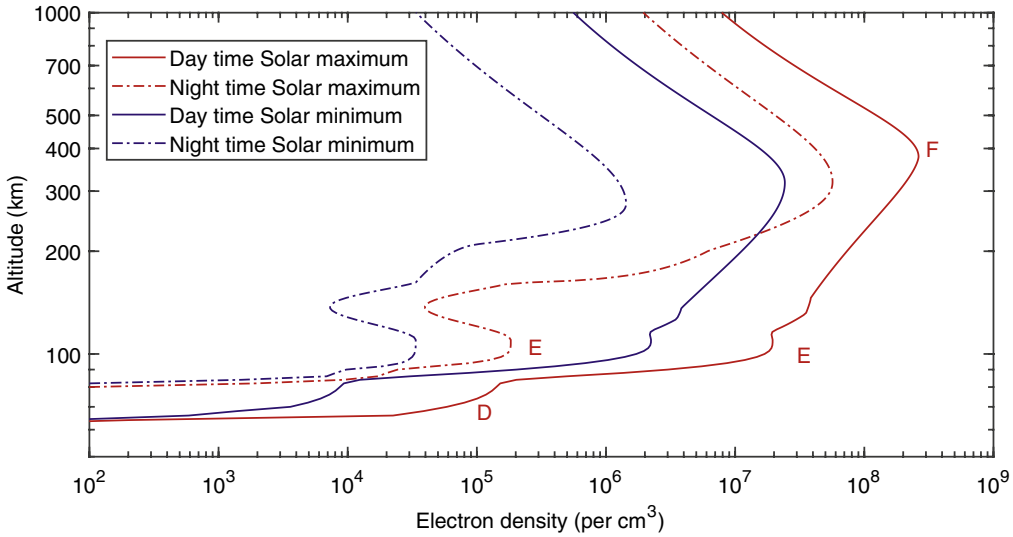

Fig. 4.1 ***Typical variation of ionospheric density values, calculated using IRI 2016 model, during high and low solar active times.***

the first layer where electric field of wave got reflected, he used the symbol "E" to describe wave's electric field. After that, at higher altitudes, a second layer was identified by him, then "F" was used as symbol for that reflected wave. Then he used the symbol "D" for a layer that he suspected at lower altitude. With time, these letters were associated with the ionospheric layers rather than electric field of those reflected waves.

The Fig. 4.1 shows the typical schematic of ionospheric layers and electron density profile. The electron density profiles for typical day and night for schematic representation are derived using the IRI model [7] available at http://irimodel.org/, for the high and low solar active times. As shown for each layer there is an altitude of maximum electron density, above and below which the ionization density tends to drop off. The ionospheric layers vary with respect to chemical composition, and particle concentration. The lowest ionospheric region is D layer whose ionization is present only during daylight hours and ranges with altitudes of about 70–90 km. The E region density extends from 90 km to about 160 km. After sunset, the electron density of E-region is diminished by a factor of 10 or more in a short time before reaching a night-time density. The F region extends upward from an altitude of about 160 km, during the day time the F-region is further distinguished into two regions F1 and F2. The F1 region has an altitude peak near 200 km and during night time this layer is absent or not distinct. The F2 region has a maximum density near 300 km during the day time and this shifts to higher altitudes at night.

The electron density of ionosphere varies with altitude and also spatially with latitude. The electron density also varies temporally with time of the day (diurnal variation), time of the year (seasonal variation) and solar cycle (11-year variation). It is obvious that

the amount of ionization in the ionosphere changes with the flux of radiation received from the sun. The ionosphere varies dramatically with geomagnetic latitudes; in particular there are three different ionospheric regions due to earth's geographic and magnetic field; they are high latitude, mid latitude and low latitude regions. The mid latitude ionosphere has obvious diurnal and seasonal variations, and this region is most modeled by many ionospheric models. At high latitudes, the ionosphere is directly coupled to the magnetospheric tail by the magnetic field lines and this connection has important consequences for high latitude ionosphere. The low latitude ionosphere region is dynamic and sensitive to plasma instabilities, and responds to the magnetospheric ring currents. The ionospheric disturbances in general are associated directly or indirectly with the events on the sun.

4.1.3 Ionosphere and its effects on Global Navigation Satellite System (GNSS)

The radio wave/signals traversing through the ionosphere experience group delay on the signal/code or information due to its encounter with the free electrons in the ionosphere. The other effects of ionosphere on the radio wave are phase advance, Doppler shift, angular refraction or bending of path, Faraday rotation of linear polarized waves, distortion of pulses transmitted. Another significant effect is due to ionospheric density irregularities that cause amplitude and phase scintillations [8]. Except ionospheric scintillation effects, all the ionospheric effects experienced by the radio signal are proportional, at least to a first order to the total number of electrons encountered by it while traversing through ionosphere [8,9]. The total electron content (TEC) is defined as the number of free electrons in a column of unit cross-sectional area along the ray path from transmitter to the receiver end [39]. Slant TEC is defined as the electron column density along an (oblique) line of sight, and slant TEC equals vertical TEC only if the line of sight goes through zenith. The measurement unit of TEC is TECU (1 TECU = 10^{16} el/m^2).

In the recent times, owing to the ever-increasing applications in space, and dependence on satellite-based navigation and such other trans-ionospheric communication systems; the study of ionosphere characteristics particularly during the space weather events such as geomagnetic storms and ionospheric scintillations has gained importance. The quality of the received signals at the GNSS receiver may be severely degraded by the density gradients in ionosphere and scintillations, affecting the accuracy and reliability of the position, velocity, and time (PVT) solution. On the other hand, the TEC and its derivatives, as well as the scintillation indices extracted from the GNSS observations, serve as the signals of opportunity for understanding and mitigating the effects in the real-time applications.

A satellite-based navigation system uses satellites to provide autonomous geo-spatial positioning. This system allows the receivers to determine their location coordinates to a

good accuracy (within a few centimeters to meters) by using time stamped radio signals transmitted by satellites. The receiver using these time stamped signals can calculate the current time to a very high precision that enables its use also for time synchronization. A satellite-based navigation system having global coverage is called as GNSS. Global coverage of such systems can be achieved by a satellite constellation of 18–30 medium earth orbit (MEO) satellites which are spread across several orbital planes. These satellites usually have orbital inclinations of >50° and about 12 hours orbital periods, so that at least 4 satellites are in the field of view at any point on globe to enable calculation of the position of the user/receiver. GNSS term is used for any satellite constellation that provides positioning, velocity, and time (PVT) services on a global or regional basis. While Global Positioning System (GPS) is one the most popular GNSS, other GNSS systems emerged to provide complementary and independent PVT capability. The other GNSS systems are BeiDou Navigation Satellite System (BDS), Galileo, GLONASS (Globalnaya Navigazionnaya Sputnikovaya Sistema), Indian Regional Navigation Satellite System (IRNSS), Quasi-Zenith Satellite System (QZSS). More information on current GNSS can be sought on webpage at link https://en.wikipedia.org/wiki/Satellite_navigation.

The signals of GNSS satellites must travel through the earth's ionosphere on their way to receivers on or near the earth's surface. Therefore, for the GNSS signals to have the precise positional accuracies, these signals must be corrected for the added ionospheric group delay and carrier phase advance. Clearly, the ionospheric TEC parameter is of great importance for maintaining accuracy in satellite ranging systems. There are many methods to determine TEC like differential Doppler, Faraday rotation, differential carrier phase, and group delay techniques. If the dual frequency GNSS receivers are used, then the ionospheric effect on the signals can be almost eliminated by taking advantage of the ionosphere's dispersive nature. On the other hand, we can also determine the error induced by the ionosphere, and reduce ionosphere parameters like TEC and irregularity strength. Using observations from GNSS receivers, the TEC estimation is more accurate than others methods, cost effective and have greater spatial coverage due to a greater number of satellites available. Thus, GNSS has become one of the powerful tools available to the ionospheric science community for studying the temporal and spatial variations of the ionosphere. In the following sections, we use GPS L1 (1575.42 MHz) and L2 (1227.60 MHz) frequencies to explain the derivation for TEC from GPS observables, as the method is very similar for any GNSS system observations using two frequencies.

4.2 Estimation of ionospheric total electron content

The effect of the ionosphere on radio waves cannot be described by simple dispersion. The ionospheric refractive index is a function of the frequency of radio wave, electron

density, and also a minor influence from intensity of earth's magnetic field. The integrated phase and group refractive indices for trans-ionosphere signal will result in a range that is different from the true geometric range between satellite and receiver. This difference in range is called ionospheric range error or ionospheric delay (in time). For carrier phase observations, this ionospheric error is negative (phase advance, shorter than geometric range), and it is positive (group delay, longer than geometric range) for the pseudorange or code observations. The ionosphere delay $\delta\rho$ experienced by the trans-ionospheric signals traversing a distance ρ, is expressed by the refractive index η integrated along the line of sight from the satellite to the receiver:

$$\delta_\rho = \int_{Rx}^{Sat} c\,\frac{dl}{\upsilon} - \rho = \int_{Rx}^{Sat} (\eta - 1)\, dl \tag{4.1}$$

where c is the speed of light in vacuum or space, and υ is the actual trans-ionospheric signal propagation velocity, Rx = receiver position and Sat = satellite position.

The equation of complex refractive index of the ionosphere is often referred to as the Appleton-Hartree formula, whose detailed derivation can be found in Davies [10]. Assuming that there is cold, collision less, magnetized plasma, the phase refractive index, η_p, can be expressed for both ordinary waves (+ sign) and extraordinary (– sign) waves as:

$$\eta_p^2 = 1 - \frac{X}{1 - \frac{Y_T^2 \sin^2\theta}{2(1-X)} \pm \left[\frac{Y_T^4 \sin^4\theta}{4(1-X)^2} + Y_L^2 \cos^2\theta\right]^{\frac{1}{2}}} \tag{4.2}$$

$$X = \frac{\omega_p^2}{\omega^2} = \frac{e^2 N_e}{4\pi^2 f^2 m\varepsilon}, Y = \frac{\omega_g}{\omega} = \frac{eB}{2\pi fm} \tag{4.3}$$

where $\omega = 2\pi f$ is the circular frequency of the carrier frequency f. The ω_p and ω_g are plasma and gyro frequencies associated with the free electrons of the ionosphere. $Y_T = Y\sin\theta$, and $Y_L = Y\cos\theta$, θ is the angle between the propagation direction of electromagnetic wave and the magnetic field B. And m = 9.109×10^{-31} kg is mass of an electron; e = 1.602×10^{-19} C, is charge of electron; $\varepsilon = 8.854 \times 10^{-12}$ F/m is the electric permittivity in free space (vacuum); N_e = number density of free electrons.

For the signals at GNSS frequencies, the frequency $\omega >> \omega_p$ (and hence $\omega >> \omega_g$), the Eq. (4.2) can be expanded into a second-order Taylor approximation and keeping the terms only up to 4th inverse power of frequency [11].

$$\eta_p = 1 - \frac{1}{2}X \pm \frac{1}{2}XY_L - \frac{1}{8}X^2 - \frac{1}{4}XY^2\left[1 + \cos^2\theta\right] \tag{4.4}$$

In the above Eq. (4.4), the positive and negative signs represent expressions for ordinary and extraordinary waves. The expression for phase refractive index η_p can be

obtained for the extraordinary signals by substituting the values of X, Y, Y_L as expressed in Eq. (4.3) in the above Eq. (4.4), we get:

$$\eta_p = 1 - \frac{e^2}{8\pi^2 m\varepsilon} \cdot \frac{N_e}{f^2} - \frac{e^3}{16\pi^3 m^2 \varepsilon} \cdot \frac{N_e B\cos\theta}{f^3} - \frac{e^4}{128\pi^4 m^2 \varepsilon^2} \cdot \frac{N_e B^2\left(1+\cos^2\theta\right)}{f^4} \tag{4.5}$$

The 2nd term in the above Eq. (4.5) accounts for more than 99.9% of the ionospheric delay calculated at GNSS frequencies [11,12,40]. At GNSS frequency bands, the 3rd, 4th, and 5th terms have the magnitude which is about 3, 5, and 6 orders less compared to the 2nd term at GNSS frequencies. Therefore, we usually use only the 1st and 2nd terms of Eq. (4.5) to get the refractive index of the ionosphere by neglecting the higher order terms; so, we get:

$$\eta_p = 1 - \frac{e^2}{8m\varepsilon\pi^2} \cdot \frac{N_e}{f^2} \tag{4.6}$$

After substituting the physical constants in the Eq. (4.6), we get:

$$\eta_p = 1 - \frac{40.3 \times N_e}{f^2} \tag{4.7}$$

Using the relation between the phase and group velocities [10], the group refractive index is expressed as:

$$\eta_g = 1 + \frac{40.3 \times N_e}{f^2} \tag{4.8}$$

after inserting Eqs. (4.7 or 4.8) in Eq. (4.1), that is, integrating along the ray path we get the delay due to ionosphere in meters as:

$$\delta_\rho = \frac{40.3}{f^2} \int_{Rx}^{Sat} N_e dl = \frac{40.3}{f^2} TEC \tag{4.9}$$

In Eq. (4.9), the term TEC is the total electron content along the ray path from receiver to satellite in a square meter cross-sectional area. For example, consider a signal from a system operating at frequency of 1 GHz traverses through TEC of 100 TEC units or 10^{18} electrons/m^2, a value (of slant TEC) that is more commonly exceeded with lower elevation angle. The 100 TEC units will produce an additional time delay of about 134 ns or 40.2 m of range error in case of satellite navigation. At a lower frequency like 100 MHz, same TEC will result in range error of above 4 km. Thus, the radio signals while traversing ionosphere experience different delays for different frequencies given by Eq. (4.9) as it is a dispersive medium. At GPS L1 frequency (1575.42 MHz), a range delay of 1 m corresponds to 6.15 TECU, or about 16.2 m range delay for 100 TEC units as per above example. Using a single frequency GPS receiver, it is difficult to estimate

the range delay without knowledge of TEC. With single frequency GPS receivers, the ionospheric models are used to correct for the ionospheric range errors to an extent. The conventional ionosphere models cannot accurately estimate TEC variations with local time, season, location, and the level of solar and magnetic disturbance. The day-to-day TEC varies from a minimum of few TEC units during night time to a day time maximum that ranges from few tens to about 100 TECU or more, depending on the location of the station, season, and solar activity ([13] and references therein). Apart from the diurnal and seasonal variations, the ionosphere density varies by substantial amounts from its average behavior during the geomagnetic storms and space weather events. The slant TEC values can go up higher depending on the elevation of the satellite.

4.2.1 TEC calculation from GPS observations

All the GPS satellites transmit the same carrier frequencies. The code modulation that is different for each satellite is used to reduce the signal interference [41,42]. These codes are known as pseudo random noise (PRN) codes, these random codes are generated using a mathematical algorithm. Since each satellite broadcasts using its own unique code combination, the satellite can be identified by its unique PRN sequence number. The raw data recorded from GNSS/GPS receiver is in various data formats. The popular format is **R**eceiver **In**dependent **Ex**change (RINEX or rinex) is an ASCII (i.e., **A**merican **S**tandard **C**ode for **I**nformation **I**nterchange) format, which is receiver independent and is mostly used for sharing data between various groups or publishing the data. Please see the link (https://igs.org/formats-and-standards/) for rinex data format definition and standards. To measure the TEC, both carrier phase and pseudo-range/code measurements from two frequencies transmitted by GNSS/GPS, that is, four observables are required. TEC is measured from GNSS/GPS using two methods, (1) from group delay or code measurements, and (2) carrier phase measurements. The TEC computation using code measurements is simple and robust [14], but the code measurements are noisier compared to carrier phase measurements. Using the difference in range delay between the two frequencies f_1 (1575.42 MHz) and f_2 (1227.6 MHz) transmitted by GPS from the same satellite to the same receiver, we can exclude all the other atmospheric delays and errors that are common for both frequencies, leaving the residue of ionospheric differential delay ($\Delta\rho$). Thus, TEC from code (pseudorange) measurements (C_1 and C_2 corresponding to frequencies f_1 and f_2) is given by

$$C_2 - C_1 = \Delta_\rho = \delta_{\rho 2} - \delta_{\rho 1} = \frac{40.3\left(f_1^2 - f_2^2\right)}{f_1^2 f_2^2} TEC \tag{4.10}$$

$$TEC_G = \frac{f_1^2 f_2^2}{40.3\left(f_1^2 - f_2^2\right)}\left(C_2 - C_1\right) \tag{4.11}$$

Similarly, we get TEC from phase measurements (L_1 and L_2) given by

$$TEC_P = \frac{f_1^2 f_2^2}{40.3\left(f_1^2 - f_2^2\right)}\left(L_1 - L_2\right) \tag{4.12}$$

The calculation of TEC from code measurements (TEC_G) are absolute estimates but noisy, of course they are biased by differential code biases (which will be addressed in the next section). And the measurements using carrier-phase are about two orders more precise compared to code measurements but these are only relative TEC (TEC_p) due to an unknown offset as the actual number of cycles of phase is not known. Therefore, usually combination of both code and phase measurements are used to overcome phase ambiguity and noise problems for an improved TEC estimate. The phase TEC measurements (TEC_p) are levelled using code TEC measurements (TEC_G) to eliminate phase ambiguity.

4.2.2 Cycle slip correction

The phase observables (L_1 and L_2) of the single PRN arc must be corrected for any cycle slips before they are used in Eq. (4.12) for derivation of phase TEC. Also seldom, researchers do the correction of cycle slips in the differential phase or phase TEC (TEC_p), wherein a cycle slip [43] is defined as a jump in differential phase TEC of more than or equal to fixed threshold TEC units (usually 1 to few TECU) in the interval defined by mostly data sampling [15,16]. Ionospheric density irregularities impact the phase of the signal; the spatially irregular phases emerging from the medium can cause constructive or destructive interference leading to increased or decreased signal amplitude [17]. These varying electron densities can cause Doppler shift that can exceed the bandwidth of the receiver's phase lock loop (PLL), which is used to continuously track the phase. In the event of phase shifts causing PLL to exceed its bandwidth, the receiver loses its lock on to signal, leading to cycle slips [18,19]. Also, during ionospheric scintillation, the destructive interference causing lower signal power can cause the receiver to lose of lock on the signals and several losses of lock events prevent will cause discontinuity in the TEC variation. Cycle slip correction requires removing the discontinuities in different phase connected arcs and producing a continuous curve. In general, the most cycle slip correction methods use either a kind of curve fitting or simple arithmetic to detect and correct the slip. The curve fitting methods are accurate but fail when there are multiple cycle slips, or during the ionospheric disturbances and/or rapid ionospheric variations. The arithmetic algorithms assume that ionosphere does not change rapidly in the data sampling interval time to correct for the offset and does a decent job at handling multiple slips. The readers can refer to a review of the popular cycle-slip correction methods and their theoretical performance, which are reported in [20].

To detect correct the cycle slips in phase TEC, the author of this chapter has adopted a simple arithmetic algorithm which is described here. The simple arithmetic progression difference with a tolerance of standard deviation of the last 10 data samples is used to detect the slip in phase TEC. The slip is corrected with an offset of the running mean of the previous 5 samples difference, given by the following equation:

$$Slip = \begin{cases} no, & (x_i - x_{i-1}) \le \sigma \\ yes, & (x_i - x_{i-1}) > \sigma \end{cases} \tag{4.13}$$

where *xi* is the phase TEC data sequence, and σ is standard deviation of the previous 10 data samples. This method has an advantage that there is no fixed threshold and it changes dynamically with data and so is suitable for any sampling interval. The false trigger of slip detection is rare as the difference with previous sample is compared against standard deviation of last 10 data values. Thus, with the occurrence of cycle slip, the difference will become significantly larger due to contribution from artificial jump as result of cycle slip. The difference in phase TEC caused by cycle slips is linearly proportional to the size of the cycle slip. This method has computational advantage compared to curve fit methods, but at times this method may produce error which is again most likely less than fraction of TEC unit, as the observed TEC with consecutive data of the satellite arc does not change more than a fraction of a TEC unit often at 30 second data interval that is popularly used in most GNSS/GPS receivers. The Fig. 4.2 shows

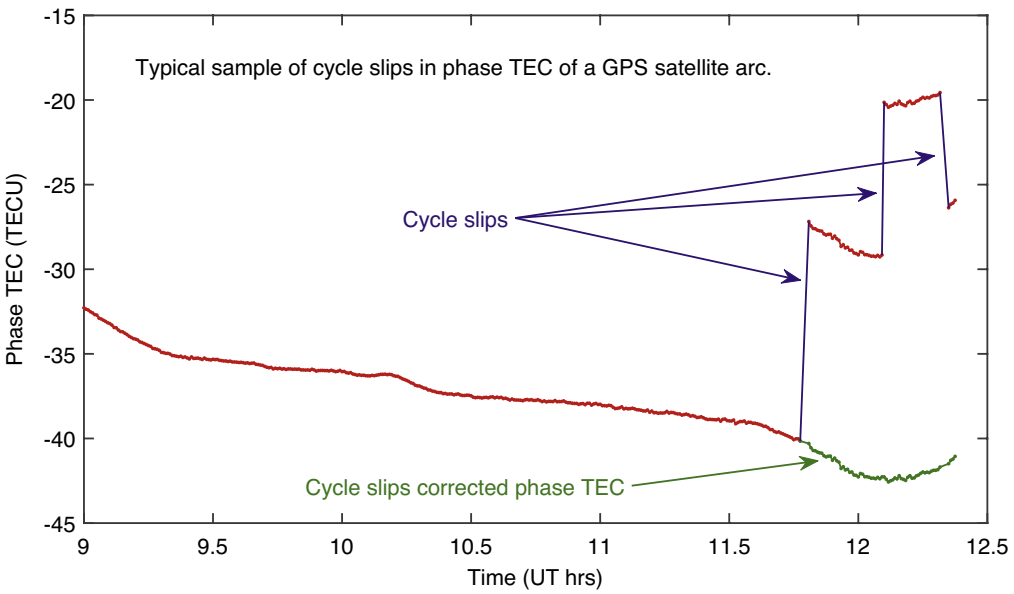

Fig. 4.2 ***A typical example showing phase TEC (in red color) with cycle slips indicated (blue color), and the phase TEC corrected for cycle slips (green color).***

a typical example for phase TEC derived from GPS satellite arc that has experienced cycle slips and the sampling rate is 30 seconds. The un-corrected phase TEC is drawn in red color with cycle slips (i.e., the jumps in phase TEC) are indicated in blue color. The phase TEC (the section with cycle slips) that is corrected for cycle slips is shown in green color line, which results in single continuous arc of phase TEC without any jumps or slips. The author has adopted and used this slip correction method in program GPS_TEC tool developed by him, that calculates TEC from rinex data [21,22] and it can be downloaded from webpage https://seemala.blogspot.com.

4.2.3 TEC leveling

The phase TEC levelling process is based on computing the baseline for each connected arc of phase measurements from a single PRN as shown in Fig. 4.3. To the level the phase TEC to the absolute and noisy group TEC, the arithmetic difference (offset) between all the TEC_P and TEC_G at each of the epochs of single satellite (or PRN) is calculated, for elevation angles >20° that are continuous in time and that form single arc. If there is a time gap, that is, the values that are from same satellite, considered as a separated arc and the same procedure is repeated for that set separately. At lower

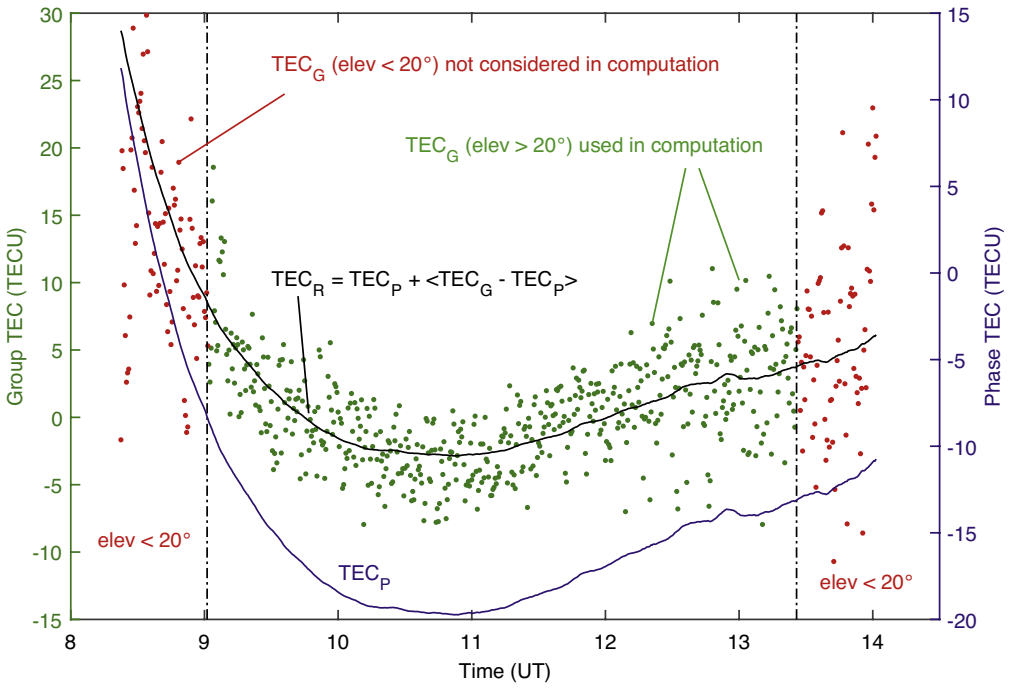

Fig. 4.3 ***Estimation of absolute TEC (REC_R) by levelling using the combination of code TEC (TEC_G) and the phase TEC (TEC_P).***

elevation angles, the group TEC values could be noisier due to multipath signals coming from horizon, ionospheric irregularities, and tropospheric scatter etc. The average offset is calculated after removing any outliers from the calculated offsets/differences. The outliers are defined as elements that are more than two local scaled median absolute deviation (MAD) [23] from the local median of selected window length (here, 1 hour is considered), as given by the following equation:

$$|y_i| = \begin{cases} x_i, & |x_i - \mu| < 2\sigma \\ outlier, & |x_i - \mu| \geq 2\sigma \end{cases} \tag{4.14}$$

where x_i is the data sequence of offsets ($TEC_G - TEC_p$) that belongs to selected window length of one hour, the μ is mean of the selected window length, and σ is its standard deviation. When the difference between the value x_i and the local mean is greater than two times the local standard deviation, then it is considered as an outlier and the data point is omitted from further calculation. The average of all the offset values from single arc of PRN, is the computed baseline value as given by the second term in the following equation is added to the phase TEC (TEC_p) values to get the slant TEC (TEC_R).

$$TEC_R = TEC_P + \sum_{i=1}^{N} \left(TEC_{Gi} - TEC_{Pi}\right) / N \tag{4.15}$$

where N is the number of data points in the single arc of the PRN. In the above equation, the ambiguity or calculated offset (second term) is considered constant for all phase TEC values for the duration of satellite pass or arc, so that it can be used to fit or level to code TEC [24,25].

The Fig. 4.3 depicts the TEC leveling process of GPS PRN 2, recorded from station "IISC," which is a part of International GNSS Service (IGS) network (https://igs.org/) for the date March 31, 2021, it was downloaded from ftp site ftp://data-out.unavco.org/pub. In the figure, code TEC (TEC_G) values are plotted as green dots for elevation angles >20° and red dots for elevation angles ≤20° which are not considered for offset baseline calculation. The phase TEC (TEC_p) values are plotted as a blue line, after adding the offset as per Eq. (4.15), the slant TEC (TEC_R) is plotted as a black line. It can be clearly seen that the final TEC_R values (shown in black line) are more precise as phase TEC and absolute without any ambiguity as code TEC; yet these slant TEC values must be processed for receiver and satellite differential code biases.

4.2.4 Vertical TEC conversion

The computed TEC_R values Eq. (4.15) shown in Fig. 4.3 as black line, are referred to as slant TEC, these values dependent on elevation angle of satellite but does not represent TEC at a particular location. The kind of unique TEC that characterizes the location will be obtained when the satellite is exactly overhead or above the location, this zenith value is called vertical TEC (VTEC). Since the GPS (in general GNSS) satellites move

in different parts of the sky and the electron content in the ionosphere varies both spatially and temporally, the slant TEC cannot used to characterize the ionospheric variation of that location; therefore, it is often desirable to calculate VTEC. During the geomagnetic storms and ionospheric irregularities, when the spatial density gradients are high, the accurate VTEC values are useful in studying the ionospheric variations which are independent of satellite elevation angles. In the conversion of slant TEC to vertical TEC, it is often assumed that the ionosphere and the plasmasphere are horizontally stratified and are spatially uniform. Further, the ionosphere is simplified to a thin layer at fixed altitude of 350–400 km above the earth's surface. This height is the effective height or of the centroid of electron density of the ionosphere, which is usually called as ionospheric pierce point height (IPP) or altitude of ionospheric intersection of the user line-of-sight to the tracked satellite as shown in the Fig. 4.4. The Fig. 4.4 illustrates the schematic of the conversion of slant TEC to vertical TEC, the assumed altitude of IPP, the geometry of the ray path from satellite to ground through the ionospheric pierce point. This method is called the thin shell (approximation) model and is widely used [26–28]. The vertical equivalent (VTEC) of measured STEC at the ionospheric piercing point (IPP) height can be determined using the ionospheric thin shell mapping function given by:

$$\mathrm{VTEC} = \left[\mathrm{STEC} - \left(\mathrm{DCB_R} + \mathrm{DCB_{Si}}\right)\right] \times \mathrm{S(E)} \tag{4.16}$$

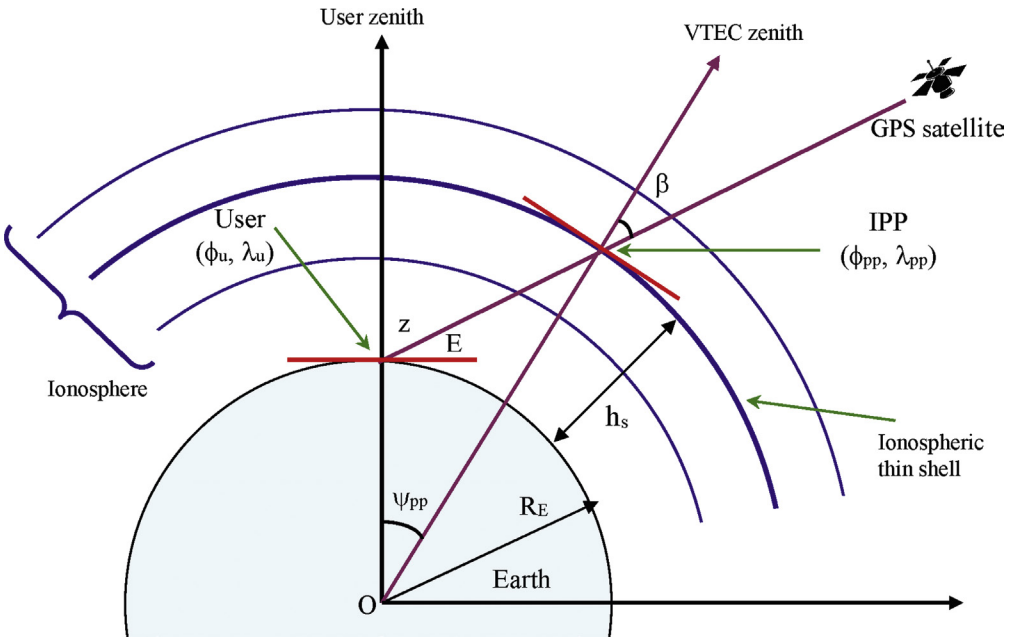

Fig. 4.4 *Schematic of Slant TEC to Vertical TEC conversion.*

where DCB_R and DCB_{Si} are the differential code biases of the receiver and "i"th satellite observed, these will be discussed in the following section. S(E) is the thin shell mapping function, whose mathematical expression is presented below:

$$S(E) = \left\{ 1 - \left(\frac{R_E \times \cos(E)}{R_E + H_{ipp}} \right)^2 \right\}^{\frac{1}{2}} \tag{4.17}$$

Here R_e is the radius of the earth (R_e = 6378 km) and E is the elevation angle of satellite with respect to receiver. H_{ipp} is the altitude of ionospheric piercing point (IPP), as mentioned it is usually assumed in the range 350–400 km, apparently based on the maximum electron density altitudes in the ionosphere.

This effective height (or IPP altitude) influences the conversion of the measured slant TEC to vertical TEC and vice-versa, it is defined by the obliquity factor that depends on the elevation angle of satellite. In the equatorial and low latitude regions, where the phenomenon like equatorial ionization anomaly (EIA) crests appear; the electron densities and the gradients are high, and the determination/assumption of a single suitable IPP altitude is more difficult. However, from the studies by Rama Rao et al. [29] the VTEC computed from STEC for different IPP altitudes ranging from 250 km to 750 km in the Indian low latitude region has revealed that resultant VTEC does not change significantly with the IPP altitude as long as the elevation angle of the satellite is greater >50°. Whereas, in the case of satellites with lower elevation angles (<50°), there is a significant departure in the computed VTEC using different IPP altitudes from both the methods. Therefore, the commonly assumed IPP altitude of 350 km can safely be used for higher elevation angles, otherwise for lower elevation angles, the local/regional average F-region peak density altitude may be used.

Using the GPS receiver's geographic latitude and longitude (ϕ_u, λ_u), the IPP location coordinates can be computed using the observed azimuth (A) and elevation angle (E) to the tracked satellite, using the single-layer ionospheric model [30]. The latitude (ϕ_{pp}) of IPP location is given by:

$$\phi_{pp} = \sin^{-1}\left(\sin\phi_u \cdot \cos\psi_{pp} + \cos\phi_u \cdot \sin\psi_{pp} \cdot \cos A \right) \tag{4.18}$$

where Ψ_{pp} is the angle subtended at the center of the earth between the user position vector and the earth projection of the pierce point, it is computed by expression:

$$\psi_{pp} = \frac{\pi}{2} - E - \sin^{-1}\left(\frac{R_E}{R_E + H_{IPP}} \cos E \right) \tag{4.19}$$

and the longitude (λ_{pp}) of the IPP is given by:

$$\lambda_{pp} = \lambda_u + \sin^{-1}\left(\frac{\sin\psi_{pp} \sin A}{\cos\phi_{pp}} \right) \tag{4.20}$$

Thus, the VTEC calculated from the measured slant TEC represents the TEC value at the IPP location (ϕ_{pp}, λ_{pp}) determined, and thus can be used in the navigation applications to study the TEC spatial and temporal behavior with a coverage limited by the elevation angle. The elevation "E" and azimuth "A" of the satellite at that epoch, with respect to the receiver location can be calculated using the position of the satellite at that time which is estimated from the ephemeris downloaded from any IGS processing center (for example: ftp://data-out.unavco.org/pub/rinex/nav/, ftp://garner.ucsd.edu/pub/nav/, http://ftp.aiub.unibe.ch/CODE/, etc.), or using the navigation file recorded by the receiver. The navigation message or the ephemeris is global to all the receivers and so the navigation file of any station can be used as long as it contains ephemeris for all satellites. For example, the program written by the author uses the station navigation file if it is present, otherwise it downloads a navigation file of predetermined station "chpi" or "cro1" and uses it for calculation of satellite's elevation and azimuth angles. The calculation of satellite's position, elevation and azimuth is beyond the scope of this chapter and the readers may refer to Strang and Borre [31].

4.2.5 Receiver and satellite differential code biases (DCBs)

As discussed in Section 4.2.3, code/pseudorange measurements are assumed to be absolute, but noisy. For this reason, usually we use combination of pseudorange and phase measurements to eliminate noise and phase ambiguity in the resultant TEC. Yet this absolute slant TEC (from Eq. 4.15) is not truly absolute. All effects such as distance of receiver to satellite, tropospheric delay, clock offsets; that are common to both frequencies are removed, but the frequency-dependent effects, like differential instrumental biases in the satellite and the receiver, and multipath are still present. The effects of multipath can be avoided with an elevation mask of 30° [32,33]. Thus, the STEC (from Eq. 4.15) still needs to be corrected for differential instrumental/code biases at satellite and receiver.

The differential code biases (DCBs), is the delay related with the different, frequency dependent times for signals in RF paths/channels at satellites and receivers. This delay bias in each signal of the two GPS/GNSS frequencies is also known as differential instrumental bias. Several meters of error can occur if the effect of the DCBs is ignored, and the estimated TEC values can even become nonphysical negative TEC [34]. For example, a 1 ns delay due to DCB causes an error of 2.85 TECU (at GPS frequencies) in TEC estimation. The DCB biases are known to vary systematically. Seasonal variations in estimated TEC errors (up to ~20 TECU) associated with receiver DCBs are observed. These variations can be related to variations in the receiver environment, like temperature [35]. Thus, the DCBs must be accounted for precise estimate of slant TEC in the Eq. (4.16) before calculation of VTEC.

The DCBs are derived by various methods; some methods are developed to calculate biases by considering more than one station and model the TEC on the double

differences of GPS observations. But, for the calculation of TEC and DCBs using single station observation, in general there are two basic approaches. The first method, the TEC is modeled by polynomial coefficients including DCBs; these unknown coefficients and DCBs in the form of linear system of equations are solved by least squares method [25,27,36,37]. In the second method, the DCB value is chosen based on searching for the true value with a constraint condition through minimizing the standard deviation [36,38]. The calculated DCBs of satellite and IGS station receiver can be directly obtained from internet from IGS analysis centers, namely, Jet Propulsion Laboratory (JPL) Pasadena, CA, USA; Center for Orbit Determination in Europe (CODE) University of Berne, Switzerland; European Space Operations Center (ESOC) of European Space Agency (ESA), Germany; and gAGE/UPC of Polytechnical University of Catalonia, Spain.

In this section, a similar approach to standard deviation minimization [36] for calculation receiver DCB using single station is described, assuming that satellite DCBs are known (or downloaded from one of IGS centers). In this technique, for a selected period, the TEC values calculated from all satellites are assumed to be close. Preferably the local post mid-night hours are chosen when the TEC is spatially uniform; so that TEC values calculated from all satellites (in that duration) will be close, as the ionosphere is mostly spatially uniform then. For this dataset, the optimum receiver DCB is selected by searching or using trail DCB values in TEC calculation and the value that minimizes the standard deviation is chosen as the DCB for that receiver/station. The minimization of standard deviation method assumes that the calculated VTEC from all satellites in view are equal satellite zenith are same. For example, if the ionosphere is horizontally homogeneous and DCBs are properly removed, the calculated VTECs from all the visible satellites must be identical. In reality, it is known that ionosphere has a horizontal gradient and vertical structure. However, if the correct DCB values are used for calculating VTEC, the scattering of VTEC values from all satellites can be safely assumed to be minimum. To reduce multipath effects an elevation mask angle of 30° is used on the dataset and this will also ensure that ionospheric spatial homogeneity to an extent as assumed in this method.

The receiver DCB is estimated by using a series of trail bias candidates and then selecting the one that has a minimum deviation of TECs with respective mean values. Mathematically, for a given range of DCB *(k)* for receiver bias to test, the standard deviation $\sigma_k(t)$ of VTECs with their mean (as discussed below) is calculated for all the 'M' satellites at each observation epoch "t," the expression is given by:

$$\sigma_k(t) = \sqrt{\frac{1}{M_n}\sum_{j=1}^{M_t}(VTEC_k^j(t) - \overline{VTEC_k}(t))^2} \tag{4.21}$$

where M_t represents the total number of satellites at epoch "t." In the Eq. (4.21), $\overline{VTEC_k}(t)$ denotes mean of all VTEC values from M_t satellites for that epoch or

selected interval. The total of standard deviations $\sigma_{Total}(k)$ is obtained for the entire day with VTEC values calculated using DCB(k) is given as

$$\sigma_{Total}(k) = \sum_{i=1}^{N} \sigma_k(t) \tag{4.22}$$

where $\sigma_k(t)$ is the sum of standard deviation values for "k"th DCB at an epoch "t," N is the number of epochs in the measurement period or selected data.

The range of DCB test values that are converted into TEC units (so to add to STEC) with a step size of 0.1 TEC units, as input for the minimization of standard deviation. Then for each of these DCB(k) values, the $VTEC_k$ values are computed using Eqs. (4.16 and 4.17), and total standard deviation $\sigma_{Total}(k)$ are calculated from above Eqs. (4.21 and 4.22). When the minimum $\sigma_{Total}(k)$ value is found, then corresponding DCB(k) is the correct estimate of receiver DCB.

This method needs a priori search range and the computation time increases with increase in search range. Also, if the given DCB range is narrower, the value of correct DCB may not be within this small range leading to an incorrect estimate of DCB. In general, most of the receiver DCB values fall within the range of –30 to 30 ns or about –90 to 90 TEC units. But, to include any peculiar receiver with high DCB value, a range of –500 to 500 TEC units will be used as trail DCB range, that could easily increase the computation time. To reduce the computation time, the variable step size was used as shown in the Fig. 4.5. Initially, a step size of 50 TECU was used for –500 to 500 TECU range (20 iterations) see Fig. 4.5A. After selecting the first minimum $\sigma_{Total}(k1)$, the range DCB(k1) ± 50 TECU with step size of 10 TECU is used again for second time (10 iterations). As shown in Fig. 4.5B, with $\sigma_{Total}(k2)$ being the second time minima selected, the third range of DCB(k2) ± 10 TECU with step size of 1.0 TECU is used for third time (20 iterations). Finally, with $\sigma_{Total}(k3)$ being the third minima (in Fig. 4.5C), another range of DCB(k3) ± 1 TECU with final step size of 0.1 TECU is used (20 iterations). The resultant selected minima $\sigma_{Total}(k4)$ will give the optimum receiver bias value DCB(k4) as shown in Fig. 4.5D. The usage of variable step size in 4 stages results in a reduced total number of iterations from 10,000 iterations to just 70 iterations instead of using uniform step size of 0.1 TECU for entire range of -500 to 500 TEC units for DCB values in Eq. (4.22).

Thus, with this usage of variable step size, the computational time is reduced by more than two orders magnitude. In addition, the data that is usually sampled at 1 to 30 s is decimated to 3 minutes, leveraging at least another one order magnitude reduction for 30 s data rate in computation time as the decimation does not the effect the estimation of optimal bias with the assumption that receiver DCB is constant throughout the day or 24 hours' time. After the estimation of optimal receiver DCB, it is used with the dataset of original sampling rate and final bias corrected STEC and VTEC values are calculated.

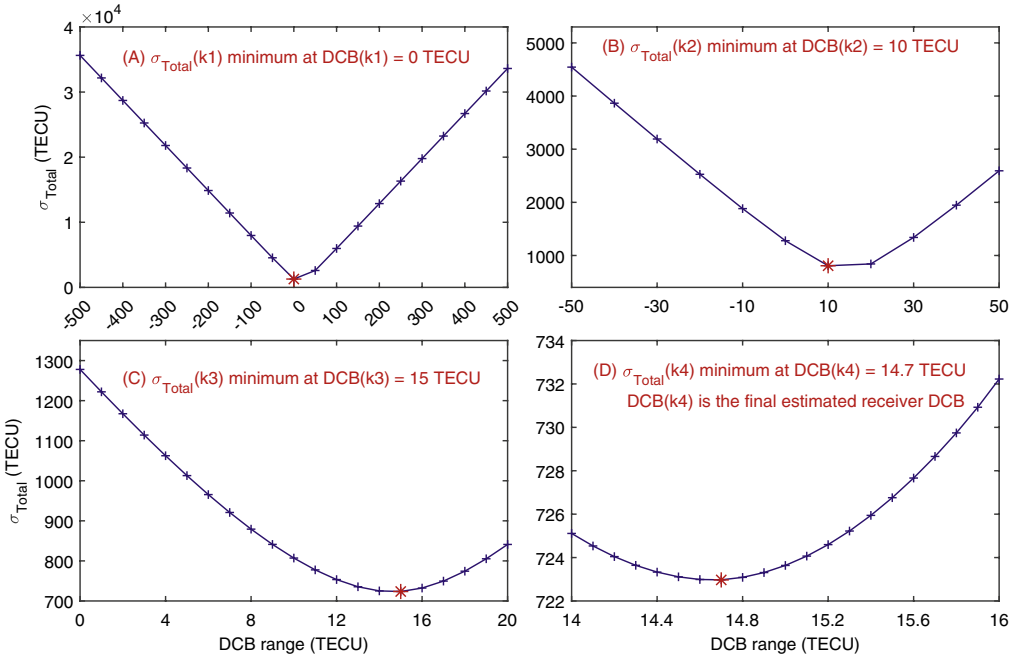

Fig. 4.5 ***Typical values σ_{Total} calculated for all epochs of day at different ranges/steps of receiver DCB ranges shown on x-axis, calculated for "IISC" station on March 31, 2021.*** This figure showcases how the minimum number of variable steps were used to reach the optimal minimum of σ_{Total}.

The distribution of vertical TEC arcs at different receiver DCB bias conditions is depicted in Fig. 4.6 by using actual data set. The data from "IISC" an IGS station is chosen, which is located at (13.02 N, 77.57 E) for the date of March 31, 2021. The absolute values of TEC are obtained by including the differential satellite biases published by the University of Bern as already mentioned in this section. The Fig. 4.6 shows VTEC values in three panels, the applied satellite biases were identical, but receiver DCBs in each of the case are different as, panel (A) the receiver DCB is over corrected or with DCB value of –20.0 TECU, we can see that VTEC (blue color) values spread throughout the day including night time and satellite arcs of hyperbolic shape; panel (B) the receiver DCB is under corrected with DCB value of 40.0 TECU, which also results in spread of VTEC (red color) values and all the satellite arcs are of parabolic shape; panel (C) the receiver DCB is optimally corrected with estimated DCB value of 14.7 TECU, we can observe that VTEC (green color) values of different satellites/PRNs are closer during night time hours and overall the most arcs are closer except at noon time where the horizontal gradients are higher.

This method of minimizing the standard deviation with variable step size and down-sampled VTEC values (to achieve 4 orders of computation efficiency) for receiver DCB estimate is currently used in GPS_TEC program tool developed by the author (Gopi

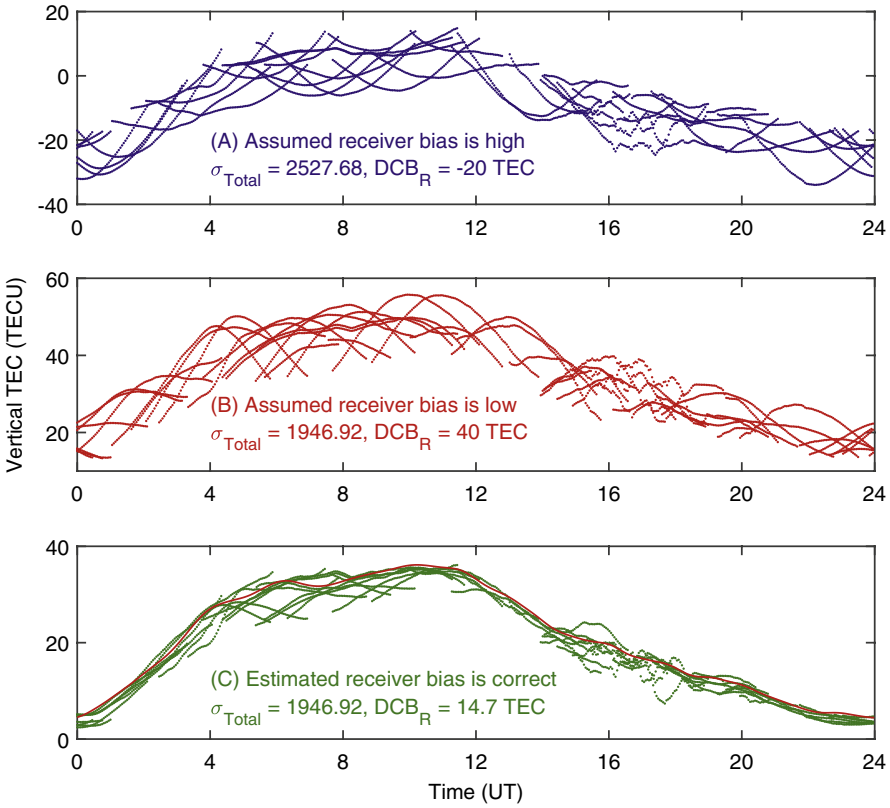

Fig. 4.6 The calculated VTEC values from observed STEC at station "IISC" for the date March 31, 2021 for different receiver bias corrections (A) when receiver bias is over corrected (B) when receiver bias is under corrected (C) the receiver bias applied is correct. The sum of the standard deviation of VTECs to their mean at all epochs of the day, is shown in each panel. The data of IISC, IGS station of date March 31, 2021 is used for VTEC derivation.

Seemala) available at webpage https://seemala.blogspot.com. Here, the VTECs are calculated by using satellite DCBs published by the University of Bern available at the link http://ftp.aiub.unibe.ch/CODE/ and receiver DCB is estimated as discussed in this section. Earlier, the first method for single station mentioned in this section, was used by the author in the program GPS_TEC, using satellite DCBs published by the University of Bern and the receiver bias is calculated by using least squares method for selected data of local night hours 02:00 to 06:00 LT [13,22]. Both these methods are practically feasible and can be used offline with an exception of assuming known satellite DCBs or that were downloaded from one of the IGS centers.

The program took a time of about 200–300 milliseconds to complete the above task of estimating the receiver DCB for 30 second daily rinex file. The total time taken by the program to complete the task of estimation of VTEC values, which includes reading

one day rinex data (30 second sampling), estimating STEC and receiver DCB, reading navigation file, calculating IPP coordinates and conversion of STEC to VTEC, and also saving the processed ASCII data and VTEC figure files, is usually less than or about 2 seconds on a simple intel processor with 2 GHz clock speed. The program is highly optimized to handle large number of rinex files at one go with built-in batch processing options, automatic download of required navigation and satellite DCB files.

The two-sigma-mean method is used to represent the mean diurnal variation of TEC at the station. This TEC diurnal variation curve is shown as red line in the Fig. 4.6C on top of individual satellite arcs of the day that are drawn in green color. The two-sigma-mean is described as follows. The mean and standard deviation of VTEC values from all satellites is calculated for all the epochs/data points in 1 minute window. Then, the values that are outside of mean ± standard deviation are eliminated. And the same process is repeated for second time, to further eliminate data points that are outside standard deviation from the mean. Now, with the remaining TEC data points in 1 minute window, the mean is calculated, this mean data value obtained over this selected window is called two-sigma-mean. The entire process is repeated for all the epochs with selected time windows, and the resultant is continuous diurnal mean TEC values with 1 minute sampling representing TEC variation for that station. These 1 minute two-sigma-mean samples are further smoothened using a used a low pass filter (with cutoff of 4 hours period) to smooth the final diurnal variation TEC values. From the Fig. 4.6C, the two-sigma-mean TEC variation in comparison with VTEC values for different satellite arcs, it can be clearly seen that the mean TEC is well represent preserving the diurnal pattern without yielding to pattern of multiple satellite arcs.

4.3 Summary

The ionospheric effect on radio signals, and the estimation of ionospheric TEC using dual frequency signals from GNSS are explained with theory. The instrumental biases or DCBs of satellite and receiver must be considered for GPS precise positioning and in calculation of TEC. The GPS data from dual frequency receiver was used to demonstrate the estimation of receiver DCB and calculation of VTEC from raw GPS observables. The chapter also explained the implementation of efficient method for the receiver DCB estimation, which is faster and sufficiently accurate for the data from GPS/GNSS receivers installed across the globe, as there is no selection of data is needed with respect to local time to ensure night time homogeneity in ionosphere. This process of TEC estimation can be extended to any GNSS raw dataset. The author has also discussed the program developed by that is available at webpage http://seemala.blogspot.com/ that has used the methods described in this chapter and that is being used by several researchers to estimate TEC data from rinex data recorded by the dual frequency GNSS receivers.

Acknowledgements

Author acknowledges IRI team for making the IRI model available online, and the IGS data archival services provided by UNAVCO, Inc. The author acknowledges Patricia Doherty, Institute for Scientific Research, Boston College for sharing the Fortran program (rinex_11.for). The author also acknowledges Institute for Scientific Research, Boston College, USA; where the author got the opportunity and initiated the work on GPS_TEC program for TEC data analysis.

References

[1] D. Martyn, Location of the currents causing the solar and lunar diurnal magnetic variations, Nature 160 (1947) 535–537. doi:10.1038/160535b0.
[2] A.E. Kennelly, On the elevation of the electrically conducting strata of the earth's atmosphere, Electr. World Eng. 39 (1902) 473.
[3] O. Heaviside, Telegraphy, Britannica 33, 10th ed., Encyclopedia Britannica, Chicago, 1902, pp. 213–218.
[4] E.V. Appleton, M.A.F. Barnett, On some direct evidence for downward atmospheric reflection of electric rays, Nature 115 (1925) 333.
[5] S. Chapman, The absorption and dissociative or ionizing effect of monochromatic radiation in an atmosphere on a rotating earth, Proc. Phys. Soc. 43 (1931) 26, doi.org/10.1088/0959-5309/43/1/305.
[6] M.C. Kelley, The Earth's Ionosphere: Plasma Physics and Electrodynamics. In: The Earth's Ionosphere: Plasma Physics and Electrodynamics, second ed., Elsevier, New York, 2009, doi.org/10.1088/0959-5309/43/1/305.
[7] D. Bilitza, B.W. Reinisch, International Reference Ionosphere 2007: Improvements and new parameters, Adv. Space Res. 42 (4) (2008) 599–609. doi:10.1016/j.asr.2007.07.048.
[8] L. Wanninger, Effects of the Equatorial Ionosphere on GPS, GPS World, Cleveland, 1993, pp. 48.
[9] J.A. Klobuchar, Ionospheric effects on GPS, in: B.W. Parkinson, J.J. Spilker (Eds.), Global Positioning System: Theory and Applications, Progress in Astronautics and Aeronautics, Volume 164, vol. 2, American Institute of Aeronautics and Astronautics INC., Washington, 1996, pp. 485–515.
[10] K. Davies, Ionospheric Radio. In: Ionospheric Radio, Peter Pergrinus Ltd., London, 1990.
[11] S. Bassiri, G. Hajj, High-order ionospheric effects on the global positioning system observables and means of modeling them, Manuscr. Geodaet. 18 (1993) 280–289.
[12] N. Jakowski, F. Porsch, G. Mayer, Ionosphere-induced ray-path bending effects in precision satellite positioning systems, Zeitschrift fur Satellitengestutzte Positionierung, Navigation und Kommunikation 1/94 (1994) 6–13.
[13] P.V.S. Rama Rao, S. Gopi Krishna, K. Niranjan, D.S.V.V.D. Prasad, Temporal and spatial variation in TEC using simultaneous measurements from the Indian GPS network of receivers during the low solar activity period of 2004–2005, Ann. Geophys. 24 (2006) 3279–3292. doi:10.5194/angeo-24-3279-2006.
[14] F. Arikan, C.B. Erol, O. Arikan, Regularized estimation of vertical total electron content from Global Positioning System data, J. Geophys. Res. 1 (18) (2003) 1469–1480 2003.
[15] Z. Liu, A new automated cycle slip detection and repair method for a single dual-frequency GPS receiver, J. Geod. 85 (2011) 171–183. doi:10.1007/s00190-010-0426-y.
[16] S. Sharma, N. Dashora, P. Galav, R. Pandey, Cycle slip detection, correction and phase leveling of RINEX formatted GPS observables, Curr. Sci. 100 (2) (2011) 205–212.
[17] P.M. Kintner, B.M. Ledvina, E.R. de Paula, GPS and ionospheric scintillations, Space Weather 5 (2007) S09003. doi:10.1029/2006SW000260.
[18] G. Blewitt, An automatic editing algorithm for GPS data, Geophys. Res. Lett. 17 (3) (1990) 199–202 .
[19] P.V.S. Rama Rao, S. Gopi Krishna, K. Niranjan, D.S.V.V.D. Prasad, Study of spatial and temporal characteristics of L-band scintillations over the Indian low latitude region and their possible effects on GPS navigation, Ann. Geophys. 24 (6) (2006) 1567–1580. doi:10.5194/angeo-24-1567-2006.

[20] S. Banville, R.B. Langley, S. Saito, T. Yoshihara, Handling cycle slips in GPS data during ionospheric plasma bubble events, Radio Sci 45 (2010) RS6007. doi:10.1029/2010RS004415.
[21] D. Okoh, G. Seemala, B. Rabiu, J.B. Habarulema, S. Jin, K. Shiokawa, et al., A neural network-based ionospheric model over Africa from Constellation Observing System for Meteorology, Ionosphere, and Climate and Ground Global Positioning System observations, J. Geophys. Res. Space Phys. 124 (2019) 10512–10532. doi:10.1029/2019JA027065.
[22] G.K. Seemala, C.E. Valladares, Statistics of total electron content depletions observed over the South American continent for the year 2008, Radio Sci 46 (2011) RS5019. doi:10.1029/2011RS004722.
[23] C. Leys, et al., Detecting outliers: Do not use standard deviation around the mean, use absolute deviation around the median, J. Exp. Social Psychol. 2013 (2013). doi:10.1016/j.jesp.2013.03.013.
[24] A. Komjathy, Global Ionospheric Total Electron Content Mapping Using the Global Positioning System (PhD thesis), Technical Report No. 188, Department of Geodesy and Geomatics Engineering, University of New Brunswick, Fredericton, New Brunswick, Canada, 1997.
[25] G.E. Lanyi, T. Roth, A comparison of mapped and measured total ionospheric electron content using Global Positioning System and beacon satellite observations, Radio Sci. 23 (4) (1988) 483.
[26] L. Ciraolo, P. Spalla, Comparison of ionospheric total electron content from the Navy Navigation Satellite System and the GPS, Radio Sci. 32 (1997) 1071–1080.
[27] D. Coco, C. Coker, S.R. Dahlke, J.R. Clynch, Variability of GPS satellite differential group delay biases, IEEE Trans. Aerospace Electr. Syst. 27 (1991) 931–938.
[28] B.D. Wilson, A.J. Mannucci, Instrumental-biases in ionospheric measurements derived from GPS data, Proceedings of ION GPS-93, Institute of Navigation, Washington, D.C., 1993.
[29] P.V.S. Rama Rao, K. Niranjan, D.S.V.V.D. Prasad, S. Gopi Krishna, G. Uma, On the validity of the ionospheric pierce point (IPP) altitude of 350km in the Indian equatorial and low-latitude sector, Ann. Geophys. 24 (2006) 2159–2168. doi:10.5194/angeo-24-2159-2006.
[30] J.A. Klobuchar, Ionospheric time-delay algorithm for single frequency GPS users, IEEE Trans. Aerospace Electr. Syst. AES-23 (3) (1987) 321–331.
[31] G. Strang, K. Borre, Linear Algebra, Geodesy, and GPS, Wellesley-Cambridge Press, Cambridge, 1997. https://klein.mit.edu/~gs/books/gps.html.
[32] M. Hernandez-Pajares, J.M. Juan, J. Sanz, Medium-scale traveling ionospheric disturbances affecting GPS measurements: Spatial and temporal analysis, J. Geophys. Res. 111 (2006) A07S11. doi:10.1029/2005JA011474.
[33] J.A.R. Rose, J.R. Tong, D.J. Allain, C.N. Mitchell, The use of ionospheric tomography and elevation masks to reduce the overall error in single-frequency GPS timing applications, Adv. Space Res. 47 (2) (2011) 276–288. doi:10.1016/j.asr.2010.05.030.
[34] E. Sardón, A. Rius, N. Zarraoa, Estimation of the transmitter and receiver differential biases and the ionospheric total electron content from Global Positioning System observations, Radio Sci 29 (3) (1994) 577–586. doi:10.1029/94RS00449.
[35] A.A. Mylnikova, Yu.V. Yasyukevich, V.E. Kunitsyn, A.M. Padokhin, Variability of GPS/GLONASS differential code biases, Results Phys. 5 (2015) 9–10. doi:10.1016/j.rinp.2014.11.002.
[36] G. Ma, T. Maruyama, Derivation of TEC and estimation of instrumental biases from GEONET in Japan, Ann. Geophys. 21 (2003) 2083–2093. doi:10.5194/angeo-21-2083-2003.
[37] R. Warnant, Reliability of the TEC computed using GPS measurements: The problem of hardware biases, Acta Geodaet. Geophys. Hungarica 32 (1997) 451–459. doi:10.1007/BF03325514.
[38] F. Arikan, H. Nayir, U. Sezen, O Arikan, Estimation of single station interfrequency receiver bias using GPS-TEC, Radio Sci 43 (2008) RS4004. doi:10.1029/2007RS003785.
[39] J.A. Klobuchar, Ionospheric effects on GPS, GPS World 2 (4) (1991) 48–51.
[40] M.M. Hoque, N. Jakowski, Estimate of higher order ionospheric errors in GNSS positioning, Radio Sci 43 (RS5008) (2008), doi:10.1029/2007RS003817.
[41] R.B. Langley, Why is the GPS signal so complex? GPS World1 (3) (1990) 56–59.
[42] B. Hofmann-Wellenhof, H. Lichtenegger, J. Collins, Satellite signal, Global Positioning System, 4th ed., Springer, New York (1997).
[43] I. Horvath, S. Crozier, Software developed for obtaining GPS-derived total electron content values, Radio Sci. 42 (20) (2007), doi.org/10.1029/2006RS003452.